

Numerical Analysis of Oxy-fuel Combustion and NO_x Formation in a Pulverized-coal Boiler

Ming-Hong Chen^{1*}

ABSTRACT

In the present study, the effect of the oxy-fuel combustion technique on the pulverized-coal boiler and NO_x formation is investigated by the proposed numerical model. The turbulence model, radiation model and combustion model are developed in the present study. Grid independent test and comparison with experimental results are conducted to validate the proposed numerical model. The air-firing and oxy-fuel conditions are calculated and compared. The results show that the oxy-fuel combustion leads to similar temperature distribution, lower wall heat flux, smaller flow velocity and longer resident time. NO_x evaluation indicates that the oxy-fuel condition is an effective way to reduce the amount of NO_x formation for the PC boiler. The results also indicate that similar thermo-conditions could be obtained by carefully manipulating the feeding conditions when switching from air-firing to oxy-fuel combustion.

Keywords: Numerical analysis, Oxy-fuel combustion, Pulverized-coal boiler.

1. Introduction

Oxy-fuel combustion technique is a carbon capture method based on the pulverized-coal (PC) boiler technology. In the oxy-fuel condition, the recycled CO₂ or CO₂/H₂O mixture is combined with pure oxygen to replace the air in the coal combustion boiler. A schematic diagram is shown in Figure 1 by the National Energy Technology Laboratory (NETL). The virtue of oxy-fuel combustion is that the product is primarily composed of CO₂ and H₂O, and the conventional PC boiler combustion condition can be obtained by controlling the concentration of the provided oxidant stream. Higher combustion temperature is attainable, which is beneficial to reducing the size of the boiler and promoting the thermal efficiency.

It also significantly reduces the formation of NO_x. Lower tail gas flow rate facilitates the purification and removal process of generated pollutants.

The first year Cost of electricity (COE) of advanced oxy-fuel combustion technologies is compared in Figure 2 with the target of Department of Energy (DOE). Although none of the current technologies meet the DOE's goal, the combined effect including all advanced technologies in the same plant will exceed the DOE target (Cumulate Case). Since none of the advanced technology is ready for commercialization, substantial research, development and demonstration are required for them to be solutions for carbon capture. In order to meet DOE's CO₂ capture goals, both the cost and performance improvements are needed in several technologies suitable to the oxy-fuel combustion.

¹ Assistant Researcher, Mechanical and System Engineering Program, Institute of Nuclear Energy Research.

* Corresponding Author, Phone: +886-3-4711400#3351, E-mail: minghongchen@iner.gov.tw

Received Date: July 17, 2020

Revised Date: September 7, 2020

Accepted Date: September 25, 2020

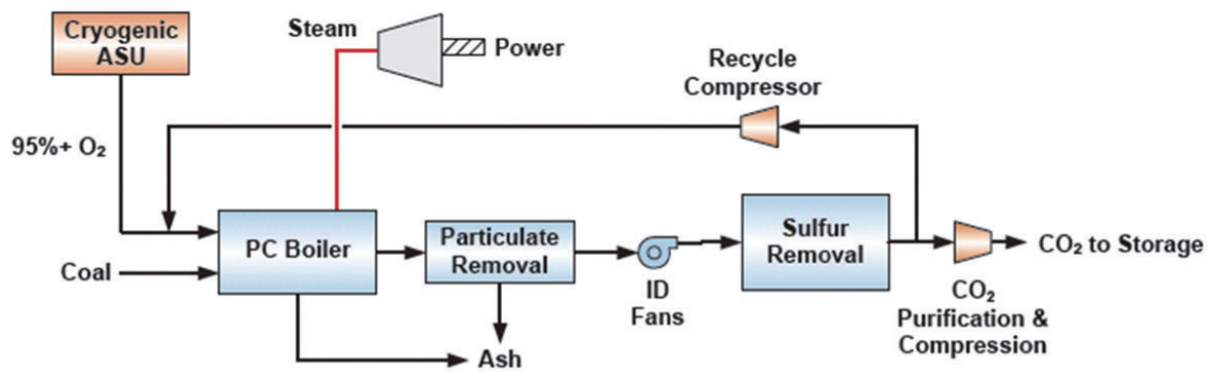


Fig. 1. Schematic diagram of the oxy-fuel combustion (NETL, 2010).

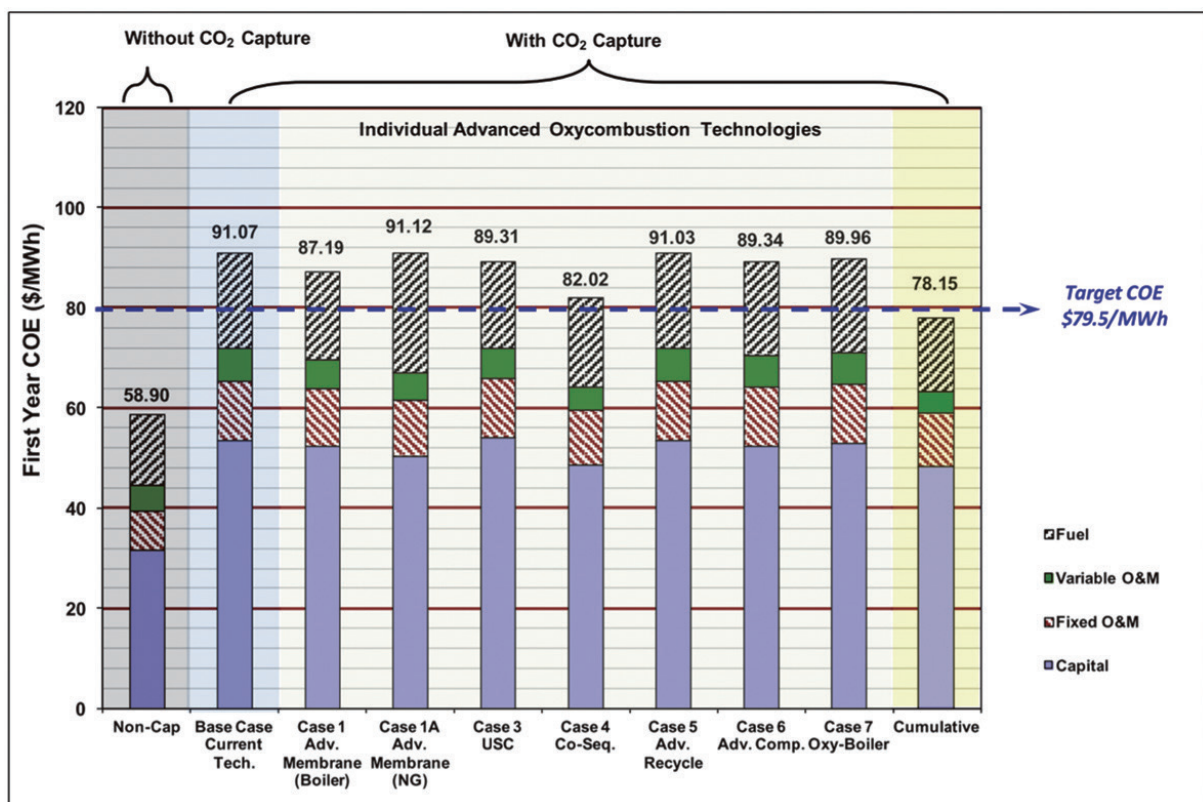


Fig. 2. Comparison of the first year cost of electricity of advanced oxy-fuel combustion technologies with the target of DOE (NETL, 2012).

Four technologies are pointed out to have the largest positive impact on oxy-fuel combustion: (1) oxygen supply, (2) sulfur-tolerant material, (3) oxy-fuel combustion boilers, (4) advanced steam condition. It was also stated that smaller oxy-fuel combustion boiler may become more effective when the sulfur-tolerant materials are available.

With the introduction of pure oxygen, higher temperature is expected and it might damage

the boiler material. Careful modification on the operational parameters should be conducted to control the combustion temperature and heat flux.

Although the study of CO₂ capture by Organization for Economic Co-operation and Development (OECD) predicted that the cost for CO₂ capture in the integrated coal gasification combined cycle (IGCC) plants will be lower than that of the post-combustion capture (traditional

PC boiler) and the oxy-fuel combustion capture by 2030, the difference is not significant (OECD, 2010). Besides, this study also indicated that the efficiency of IGCC plant with CO₂ capture will reach 48% of lower heating value (LHV) at 2030, which is higher than those by the two other methods (44%). The oxy-fuel approach, however, has grasped much attention due to the virtues mentioned above and the potential to directly retrofit the present power plants. Therefore, the overall cost could be lower than that of a newly reconstructed IGCC system, and the oxy-fuel technique can be treated as an updated version of the present technique. For power generation companies, the impact of introducing the oxy-fuel method on the present staff is lower than that of the IGCC plant.

Some studies conducted numerical analyses of the oxy-fuel combustion issues. For example, Chui *et al.* (Chui *et al.*, 2004) used CANMET to build the numerical model to investigate the oxy-fuel combustor. The results showed that the NO_x formation was 70% lower for the case using oxy-fuel than that of the air-firing condition, and the better combustion characteristics was also obtained. The proposed numerical model could be employed in the preliminary evaluation in the design of the combustor enlargement. Backreedy *et al.* (Backreedy *et al.*, 2006) proposed a numerical model for a 1 MW oxy-fuel combustor to evaluate the formation of NO_x by using several kinds of coal, analyze the unburned coal, and investigate the precision and sensitivity of the coal combustion model. Nikolopoulos *et al.* (Nikolopoulos *et al.*, 2011) developed a three-dimensional model to investigate the effect of air-firing, partial oxy-fuel and oxy-fuel firing conditions on the combustion of a pulverized-coal boiler. In the air-firing condition, the calculated combustion and the

NO_x formation were consistent with measured experimental results. The partial and full oxy-fuel firing condition also led to consistent results with experimental data. It was also mentioned that the proposed model, including the particle trajectory, reaction rate and NO_x formation, could be implemented in the development of large-scale demo plants. Porter *et al.* (Porter *et al.*, 2010) investigated the radiation model employed in the oxy-fuel combustor. The radiation model of P1 and discrete ordinate method (DOM) were investigated and consistent results with benchmark data were observed. The results also showed that using the gray mode in the simulation of the oxy-fuel combustor leads to significant error. Therefore, the non-gray radiation mode should be implemented to obtain reliable results in the evaluation of the radiation. Edge *et al.* (Edge *et al.*, 2011) investigated the effect of the large eddy simulation (LES) and the RANS (Reynolds-averaged Navier-Stokes) turbulence model on the oxy-fuel combustion. The results showed that the LES model was superior to the RANS model in the prediction of the recirculation zone and flame properties. Jovanovic *et al.* (Jovanovic *et al.*, 2011) conducted the experiment and simulation of the ignition of the pulverized-coal combustion in the oxy-fuel condition. By comparing with experimental results, the defaulted parameters of the ignition and combustion sub-model in FLUENT were adjusted to fit the experimental results. Arias *et al.* (Arias *et al.*, 2008) investigated the oxy-fuel combustion characteristics of biomass (Eucalyptus) blended with coal (20% in maximum). The NO_x formation, however, was not evaluated. Al-Abbas *et al.* (Al-Abbas *et al.*, 2011) examined the effect of the oxy-fuel combustion (replacing N₂ of air by CO₂), while the NO_x formation was not evaluated. Choi and Kim (Choi and Kim, 2009) developed a

numerical model and NO_x formation sub-model for a 500 MW scale PC boiler. The calculated results showed significant relations on the NO_x formation, combustion process, furnace temperature, and species concentration within the boiler. The over-firing air (OFA) condition effectively decreased the NO_x formation. The decrease of the fuel NO_x was due to the reduction of the contact of nitrogen and fuel, while it was the reduction of temperature for the decrease of the thermal NO_x . This study would be a suitable case as the benchmark for the air-firing furnace condition to investigate the formation of NO_x . One step further could be conducted by introducing the oxy-fuel condition into the 500 MW scale PC boiler and investigate its effect on the formation of NO_x . Álvarez *et al.* (Álvarez *et al.*, 2012) evaluated the NO_x formation for the condition of 21% O_2 /79% N_2 and 21% O_2 /79% CO_2 . The results showed that replacing N_2 by CO_2 led to lower NO_x formation. Habermehl *et al.* (Habermehl *et al.*, 2012) evaluated the NO_x emission for the air and oxy-fuel condition. The results indicated that the NO_x formation is reduced when switching to the oxy-fuel condition.

Clements *et al.* (Clements *et al.*, 2015) evaluated the applicability of the full-spectrum k-distribution (FSK) model for the radiation of Computational Fluid Dynamics (CFD) model in the oxy-fuel combustion process. Good agreement was observed in the examined cases. However, the inaccuracy was addressed for the case of large variation of CO_2 and H_2O ratio. Clements *et al.* (Clements *et al.*, 2015) conducted the comparison of LES and Reynolds-averaged Navier Stokes (RANS) model for the calculation of a 250 kW oxy-fuel combustion furnace. The predictions were validated against experimental data for both air and oxy-fuel conditions. Two radiations were introduced, namely the weighted sum of grey gases

(WSGG) and full-spectrum correlated k (FSCK) model. Results showed that small variation was observed in the choice of radiation for the RANS model, while better agreement was obtained in the case of LES model. Ma *et al.* (Ma *et al.*, 2017) employed the Large Eddy Simulation (LES) model for the gas phase turbulence the oxy-fuel spray jet flames. Two-phase flow was solved by the Eulerian-Lagrangian method. Agreement with the cited experimental data was observed. Yang *et al.* (Yang *et al.*, 2018) evaluated the thermal radiation for the small and pilot-scale furnace. The scales of the investigated furnaces were 250 kW and 35 MW, respectively. Employed radiation models were FSCK and WSGG. Good agreement was observed against the experimental results. Liang *et al.* (Liang *et al.*, 2020) investigated the formation mechanism of NO_x by a lab-scale oxy-fuel combustion reactor and numerical model. Good agreement between the experimental and numerical results was obtained. Parametric study showed that the amount of NO increased by 1.56 times when the temperature increased from 700°C to 1,100°C. They also concluded that the intermediate species, i.e., NCO, HNO, and NH would significantly affect the formation of NO_x .

From the above literature survey, it is shown that the studies of the oxy-fuel boiler are conducted on the comparison between the oxy-fuel condition and the traditional combustion, NO_x reduction operation, turbulence model, modification of the combustion model, radiation and the fundamental combustion phenomena. The behavior of NO_x formation is still challenging since it will vary greatly among the scale of the investigated reactor. Empirical parameters of NO_x formation model suitable for the lab-scale facility may not be applicable for the pilot or commercial scale furnace. Numerical analysis model can be

employed to investigate the difference between the oxy-fuel and the traditional air-firing conditions, evaluate the NO_x formation and conduct the optimization of the operating conditions. This analyzing capability is essential for the development and operating condition test of the oxy-fuel boiler. Therefore, the numerical model for the oxy-fuel boiler is developed in the present study. The NO_x model is also developed to evaluate the formation of NO_x for the air-firing and oxy-fuel conditions.

2. Physical and Numerical Model

In the present study, the numerical models including the turbulence model, coal-particle injection model, chemical reaction model, radiation model, devolatilization and combustion model are built for the investigation of a pulverized-coal boiler. The Renormalization Group (RNG) k - ε is used to predict the turbulent flow in the boiler instead of the standard k - ε model, due to the superiority for the swirling flow (Fan *et al.*, 2001). The track of the pulverized-coal particles are described by the Lagrangian frame. The dispersion of the coal particle due to the turbulence effect is evaluated by the stochastic tracking model, which is able to model the effect of instantaneous turbulence velocity fluctuation on the particle trajectory. The effect of the discrete phase on the continuous gas flow is updated every 25 iterations.

The discrete ordinates (DO) model is employed for the evaluation of the radiation. Absorption coefficients of the gaseous species are evaluated by the weighted-sum-of gray-gases model (WSGGM) (Raithby and Chui, 1990). The two-competing-rates model is used for the devolatilization of the pulverized-coal particles (Kobayashi *et al.*, 1977), while it is kinetics/

diffusion-limited model for the char combustion (Field, 1969).

2.1 Combustion model

The combustion is evaluated by the non-premixed combustion model, and the instantaneous thermo-chemical state of the fluid is related to a conserved scalar quantity known as the mixture fraction, f . The mixture fraction can be written in terms of the atomic mass fraction as (Sivathanu and Faeth, 1990):

$$f = \frac{Z_i - Z_{i,ox}}{Z_{i,fuel} - Z_{i,ox}} \quad (1)$$

where Z_i is the elemental mass fraction for element, i . The subscript ox denotes the value at the oxidizer stream inlet and fuel denotes the value at the *fuel* stream inlet.

The species equations can be reduced to a single transport equation for the mixture fraction, f , under the assumption of equal diffusivities. The reaction source terms in the species equations cancel one another eventually, and thus f is a conserved quantity. Although the assumption of equal diffusivities is problematic for laminar flows, it is generally acceptable for turbulent flows where turbulent convection overwhelms molecular diffusion. The Favre mean (density averaged) mixture fraction equation is

$$\frac{\partial}{\partial t}(\rho \bar{f}) + \nabla \cdot (\rho \bar{v} \bar{f}) = \nabla \cdot \left(\frac{\mu_t}{\sigma_f} \nabla \bar{f} \right) + S_m \quad (2)$$

The source term S_m is due to the mass from reacting particles (i.e., coal) into the gas phase (kg/s). In addition to solving the Favre mean mixture fraction, the conservation equation for the mixture fraction variance is also be solved (Jones and Whitelaw, 1982), which is given as:

$$\begin{aligned} & \frac{\partial}{\partial t}(\rho \overline{f'^2}) + \nabla \cdot (\rho \bar{v} \overline{f'^2}) \\ &= \nabla \cdot \left(\frac{\mu_t}{\sigma_f} \nabla \overline{f'^2} \right) + C_g \mu_t (\nabla \bar{f})^2 - C_d \rho \frac{\varepsilon}{k} \overline{f'^2} \end{aligned} \quad (3)$$

The values for the constants σ_i , C_g , and C_d are 0.85, 2.86, and 2.0, respectively. The probability density function (PDF), written as $p(f)$, can be thought as the fraction of time that the fluid spends in the vicinity of the state f . It is written mathematically as follows:

$$p(f)\Delta f = \lim_{T \rightarrow \infty} \frac{1}{T} \sum_i \tau_i \quad (4)$$

where T is the time scale and τ_i is the amount of time that f spends in the Δf band. The shape of the function $p(f)$ depends on the nature of the turbulent fluctuations in f . The shape of the assumed PDF, $p(f)$, is described by the mathematical function, i.e., the β -function. The β -function PDF shape is given as:

$$p(f) = \frac{f^{\alpha-1}(1-f)^{\beta-1}}{\int f^{\alpha-1}(1-f)^{\beta-1} df} \quad (5)$$

where

$$a = \bar{f} \left[\frac{\bar{f}(1-\bar{f})}{\bar{f}'^2} - 1 \right] \quad (6)$$

$$\beta = (1-\bar{f}) \left[\frac{\bar{f}(1-\bar{f})}{\bar{f}'^2} - 1 \right] \quad (7)$$

The PDF shape of $p(f)$ is a function of the mixture fraction and the mixture fraction variance only. Thus, through solving the conservation equations for the mean mixture fraction and the mixture fraction variance at each point in the flow

field, the assumed PDF shape can be computed and used as the weighting function to determine the mean values of species mass fractions, density, and temperature. Significant computational time can be saved by computing these integrals once, storing them in a look-up table, and retrieving them during the iteration.

2.2 Investigated PC boiler

The schematic diagram of the investigated PC boiler based on the cited reference (Choi and Kim, 2009) is shown in Figure 3.

The height of the furnace section is about 51 m, and both the width and depth are 16.5 m. Twelve burners are installed at four corners and three sections (Section A, B, and C) with a tilted angle for generating a swirl-firing configuration in the furnace to enhance mixing and promote combustion. The feeding module is modeled by two coal and three air-feeding inlets, while it is modeled as one feeding inlet for both coal and air in the cited study (Choi and Kim, 2009). The OFA ports is closed in the present study to be consistent with the experimental condition (Choi and Kim, 2009).

2.3 Operating conditions

The combusted, high-temperature flue gas

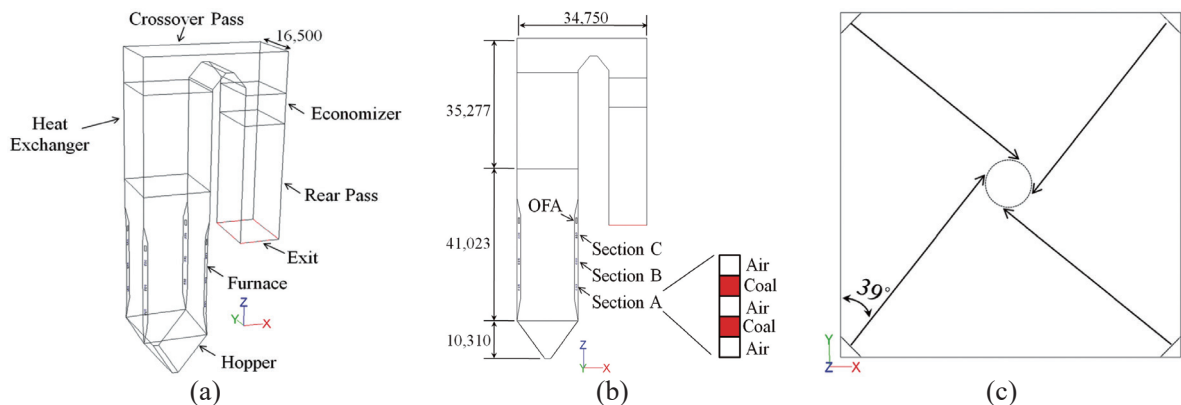


Fig. 3. Schematic diagram of the (a) pulverized-coal boiler, (b) x-z cross section, (c) x-y cross section at inlet, with unit of mm (by author).

goes through the furnace to the sequential heat exchanger and the economizer to provide the thermal energy. The mass flow rate and temperature of coal and air introduced to the furnace are shown in Table 1.

Table 1. Feeding conditions of the boiler (Choi and Kim, 2009)

	Mass flow rate (kg/s)	Temperature (K)
coal	1.994	355
air	18.944	588

The employed coal is the pulverized Bituminous coal and its high heating value is 28.28 MJ/kg (dried basis). The relevant coal properties are listed in Table 2.

Table 2. Employed coal properties (Choi and Kim, 2009)

Ultimate analysis (%) (DAF)	C	81.9
	H	5.1
	O	10.3
	N	1.7
	S	1.0
Proximate analysis (%)	Volatile	29.5
	Fixed carbon	54.7
	Ash	15.8
HHV (MJ/kg)	Dried basis	28.286
Particle diameter (μm)	Minimum	6
	Maximum	132
	Mean	44
Particle distribution	Rosin-Rammler	
Spread parameter (-)	1.15	
Density (kg/m ³)	1,300	

The heater and economizer are modeled as porous media by considering the effective pressure drops using equivalent inertial resistances (Díez *et al.*, 2008; He *et al.*, 2004; Belosevic *et al.*, 2006). The measured heat sinks are also incorporated for these two sections. The inertial resistance

coefficients are evaluated by considering the tube arrangement, geometry, flow configuration and pressure drop within each section. The inertial resistance coefficients in the primary flow direction (z-direction) and the heat absorption of heater and economizer are shown in Table 3.

Table 3. Porous property and heat sink (Choi and Kim, 2009)

	Inertial resistance coefficient			Heat absorption [MW]
	x	y	z	
Heat Exchanger	50	50	0.5	487
Economizer	50	50	6.2	57

The total heat transfer measured in these sections is about 544 MW and the furnace wall temperature is 700 K (Choi and Kim, 2009). The furnace wall emissivity is chosen as 0.6 due to the closest predicted temperature to the measured value (Choi and Kim, 2009).

2.4 NO_x model

The NO_x formation of the investigated PC boiler is evaluated by the following models. It is assumed that the concentration of NO_x is very low and its impact on the coal combustion is negligible. The amount of NO_x production is evaluated by the predicted temperature and species distribution after the calculation of coal combustion. There are three primary mechanisms of the NO_x formation, i.e., thermo NO_x, fuel NO_x, and prompt NO_x. The convection, diffusion, production and consumption of NO species, namely NO, NO₂, N₂O, are considered by solving the transported equations of those NO species. Additional transport equations are also solved for the intermediate species (HCN and NH₃) of the fuel NO_x sources.

Thermal NO_x formation is a high-temperature process in fuel-lean condition. Temperature and

the residence time are two main factors affecting the formation of thermo NO_x . In the present study, the formation of thermal NO_x is evaluated by the extended Zeldovich mechanism as:



where k_f and k_r are the forward and reverse reaction rates. The rate related parameters are adopted from the study of Hanson and Salimian (Hanson and Salimian, 1984). The transport equation of thermo NO_x mechanism is:

$$\frac{\partial}{\partial t}(\rho Y_{\text{NO}}) + \nabla \cdot (\rho \vec{v} Y_{\text{NO}}) = \nabla \cdot (\rho D \nabla Y_{\text{NO}}) + S_{\text{NO}} \quad (11)$$

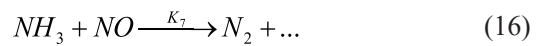
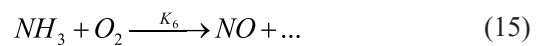
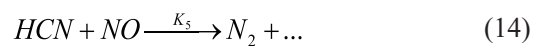
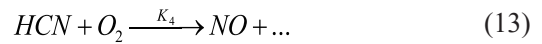
where Y_{NO} is the mass fraction of NO in gas phase, D is the effective diffusivity coefficient (m^2/s), S_{NO} is the source term for NO. The net rate of NO formation by equations (8)-(10) is described as:

$$\frac{\partial [\text{NO}]}{\partial t} = k_{f,1}[\text{O}][\text{N}_2] + k_{f,2}[\text{N}][\text{O}_2] + k_{f,3}[\text{N}][\text{OH}] - k_{f,1}[\text{NO}][\text{N}] - k_{f,2}[\text{NO}][\text{O}] - k_{f,3}[\text{NO}][\text{H}] \quad (12)$$

The units of all concentrations are $\text{g-mol}/\text{m}^3$. The partial equilibrium approach (Warnatz, 2001) is employed in the calculation of the concentrations of O, H, and OH.

For the fuel NO_x , it is assumed that the fuel nitrogen is distributed between the volatile matters and char. The fraction of nitrogen in the volatile species and char should be specified separately, since the nitrogen does not equally distribute between the volatile species and char. The tracking of the intermediate species of nitrogen is essential for the fuel NO_x evaluation, and it is appropriate to assume that the HCN and NH_3 are the primary intermediate species (Choi and Kim,

2009). Therefore, the assumption is adopted that 90% of nitrogen via volatile species converts to HCN and the rest converts to NH_3 (Winter *et al.*, 1996). In the fuel-lean environment, HCN and NH_3 transform to NO, while they transform to N_2 in fuel-rich conditions, based on the following reaction mechanisms (Soete, 1975):



The rate constants of k_4 - k_7 are adopted from the study of Soete (Soete, 1975). The transport equations to be solved of these intermediate species are:

$$\frac{\partial}{\partial t}(\rho Y_{\text{HCN}}) + \nabla \cdot (\rho \vec{v} Y_{\text{HCN}}) = \nabla \cdot (\rho D \nabla Y_{\text{HCN}}) + S_{\text{HCN}} \quad (17)$$

$$\frac{\partial}{\partial t}(\rho Y_{\text{NH}_3}) + \nabla \cdot (\rho \vec{v} Y_{\text{NH}_3}) = \nabla \cdot (\rho D \nabla Y_{\text{NH}_3}) + S_{\text{NH}_3} \quad (18)$$

where Y_{HCN} and Y_{NH_3} are mass fractions and S_{HCN} and S_{NH_3} are source terms of HCN and NH_3 , respectively. The source terms in equations (11), (17), and (18) are determined by:

$$S_{\text{HCN}} = S_{p,vc,\text{HCN}} + S_{\text{HCN}-1} + S_{\text{HCN}-2} \quad (19)$$

$$S_{\text{NH}_3} = S_{p,vc,\text{NH}_3} + S_{\text{NH}_3-1} + S_{\text{NH}_3-2} \quad (20)$$

$$S_{\text{NO}} = S_{\text{char},\text{NO}} + S_{\text{NO}-1} + S_{\text{NO}-2} + S_{\text{NO}-3} \quad (21)$$

$$S_{p,vc,\text{HCN}} = S_{\text{vol},\text{HCN}} + S_{\text{char},\text{HCN}} \quad (22)$$

$$S_{p,vc,\text{NH}_3} = S_{\text{vol},\text{NH}_3} + S_{\text{char},\text{NH}_3} \quad (23)$$

where $S_{\text{HCN}-1}$, $S_{\text{HCN}-2}$, S_{NH_3-1} , S_{NH_3-2} , $S_{\text{NO}-1}$, $S_{\text{NO}-2}$ are mass consumption rates of corresponding

species (Millares, 1992). The source terms from the volatile and char in equations (19)-(23) are evaluated as:

$$S_{vol,HCN} = \frac{S_{vol} Y_{N,vol} MW_{HCN}}{MW_N V} \quad (24)$$

$$S_{vol,NH_3} = \frac{S_{vol} Y_{N,vol} MW_{NH_3}}{MW_N V} \quad (25)$$

$$S_{char,HCN} = \frac{S_c Y_{N,char} MW_{HCN}}{MW_N V} \quad (26)$$

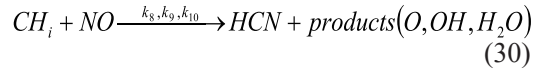
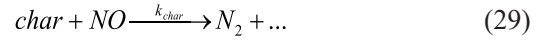
$$S_{char,NH_3} = \frac{S_c Y_{N,char} MW_{NH_3}}{MW_N V} \quad (27)$$

$$S_{char,NO} = \frac{S_c Y_{N,char} MW_{NO}}{MW_N V} \quad (28)$$

where S_{vol} is the source of volatile from the coal particle of discrete phase to continuous phase (kg/s), S_c is the char burnout rate (kg/s), $Y_{N,vol}$ is the mass fraction of nitrogen in volatile, $Y_{N,char}$ is the mass fraction of nitrogen in char, MW_i is the molecular weight of i^{th} species, and V is the cell volume (m³).

The heterogeneous reaction of char is mainly an adsorption process, and its reaction rate is directly proportional to the pore surface area. The pore surface area is known as the Brunauer-Emmett-Teller (BET) surface area due to pioneered researchers on the adsorption theory (Brunauer, 1943). The pore (BET) surface areas ranges from 1.0×10^6 to 2.0×10^6 m²/kg, depending on the microscopic structure of the commercial adsorbents, while it is typically 25,000 m²/kg

for coal (ANSYS, 2013). It is assumed that the nitrogen within char will be converted to NO (Millares, 1992), and the sources of HCN and NH₃ from char are zero. The reduction of NO via reactions with char and hydrocarbons are also considered as:



The rate constants of the re-burn process of NO are employed from Bowman (Bowman, 1991). The formation of the prompt NO_x is not considered since it is significant under the low-temperature or fuel-rich environment only. In the present high-temperature and fuel-lean conditions, the amount of prompt NO_x is negligible (Choi and Kim, 2009).

3. Results and discussion

3.1 Grid independent test and model validation

Three computational meshes (0.21 M, 0.32 M, and 0.49 M) are examined for the grid-independent test. Four physical properties, i.e., the furnace outlet temperature, furnace wall heat flux, CO₂ and O₂ mole fractions at the outlet of the furnace, are compared in the grid-independent test. As shown in Table 4, the difference of the wall heat flux between the grid of 0.21 M and 0.32 M is about

Table 4. Comparison of the grid independent test (by author)

	0.21 M	0.32 M	0.49 M
T _{out_Furnace} (K)	1504	1491	1489
Heat Flux (W)	5.19E+08	5.28E+08	5.28E+08
Mole fraction of CO ₂ (%)	16.65	16.80	16.60
Mole fraction of O ₂ (%)	1.07	1.0	1.10

1.7%, while it reduces to 0.2% when increasing the grid to 0.49 M. The difference of the furnace outlet temperature between the grid of 0.21 M and 0.32 M is about 0.5%, while it reduces to 0.13% when increasing the grid to 0.49 M. Consistent mole fractions of CO_2 and O_2 are also observed in this comparison. Therefore, the grid of 0.32 M is adequate to provide the reliable computational results in the present study, and it is employed in the following investigation.

The calculated results by the proposed model are compared with the experimental value in Table 5. Temperature difference is about 0.4%, and it is about 2.5% for heat flux of the furnace. The difference of outlet species is about 1.4%, which is comparable with relevant studies in literature [0.5% (Choi and Kim, 2009), and 1.8% (Kuang *et al.*, 2013)]. The results by the proposed model are consistent well with the experimental data, validating the proposed numerical model.

3.2 Comparison of the air-firing and the oxy-fuel conditions

In the numerical modeling, the oxy-fuel condition is employed by replacing N_2 of air with CO_2 . The comparison of the air-firing and the oxy-

fuel combustion is shown in Table 6. The results show that the oxy-fuel condition leads to slightly higher temperature ($\sim 7\text{K}$) at furnace exit and 4.2% lower for the wall heat flux. The variation of O_2 is not significant, while the fraction of CO_2 increases from 17% to 90%.

The temperature distributions are presented in Figure 4. Primary combustion is observed within the furnace zone with vortex generated via the tilted burner on four corners. Significant temperature reduction is observed in the section of heat exchanger by the designated heat absorption, and it is minor in the section of economizer section with much smaller heat absorption. In overall, the temperature distribution for the case of oxy-fuel and air-firing are similar.

The distribution of O_2 is compared at Figure 5. Higher O_2 mole fraction is observed near the feeding region for both investigated cases, and it drastically decreases due to the combustion. It is also shown that the fraction of O_2 within the furnace is relatively higher when employing the oxy-fuel condition, especially near the feeding region. The average values at outlet of the boiler, however, are comparable for both investigated cases.

Table 5. Comparison of the calculated results with experimental values (by author)

	Measured (Choi and Kim, 2009)	Present study
$T_{\text{out Furnace}}$ (K)	1485	1491
Heat Flux (W)	5.15E+08	5.28E+08
Mole fraction of CO_2 (%)	15.5	16.8
Mole fraction of O_2 (%)	2.5	1.0

Table 6. Comparison of the air-firing and oxy-fuel condition (by author)

	Air-firing	Oxy-fuel
$T_{\text{out Furnace}}$ (K)	1491	1498
Heat Flux (W)	5.28E+08	5.06E+08
Mole fraction of CO_2 (%)	16.79	89.67
Mole fraction of O_2 (%)	1.0	1.40

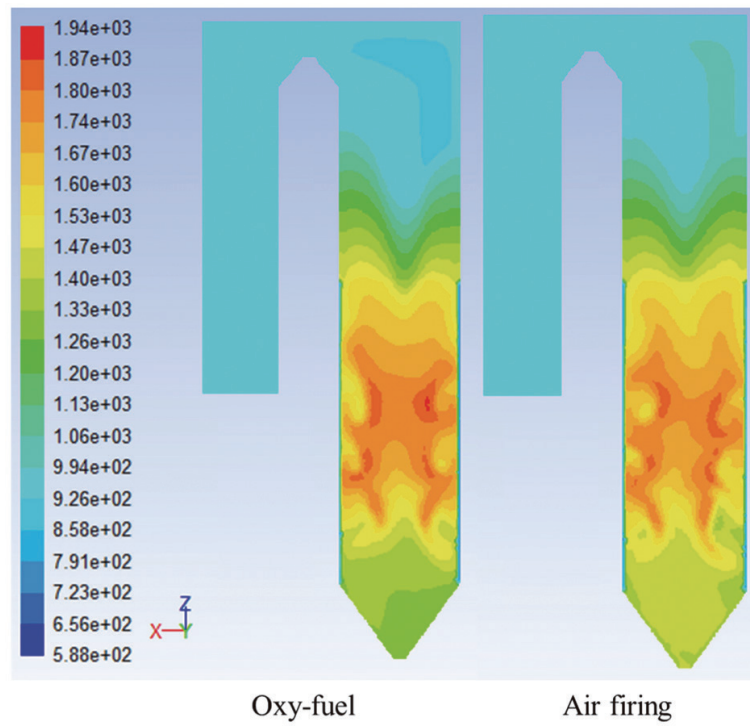


Fig. 4. Temperature distribution of oxy-fuel and air-firing condition (Unit: K) (by author).

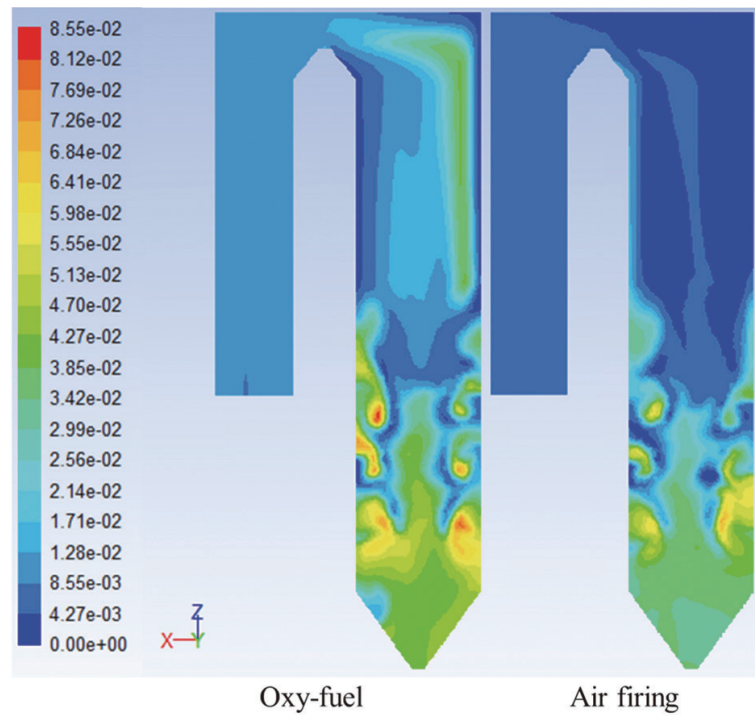


Fig. 5. O₂ distribution of oxy-fuel and air-firing condition (Unit: mole/mole) (by author).

For CO₂, the species distributions are compared at Figure 6. This comparison shows that there are six regions with minimum CO₂ fraction near the feeding zone and those are corresponding to the regions with the maximum O₂ fraction.

Those six regions with extreme species fraction are due to the vortex flow within the furnace generated by the tilted feeding design. The fraction of CO₂ increases gradually with the combustion and it reaches the maximum value when leaving the

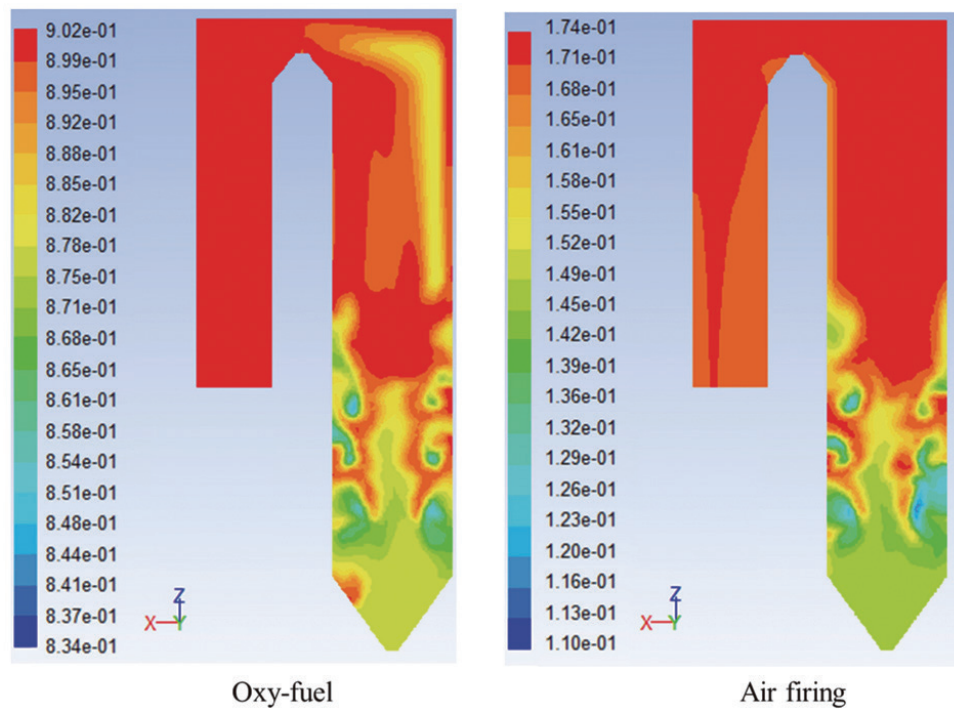


Fig. 6. CO₂ distribution of oxy-fuel and air-firing condition (Unit: mole/mole) (by author).

furnace. The maximum value is about 90% for the oxy-fuel combustion, and it is about 16% for the air-firing condition.

The cross-sectional distribution of velocity

is shown in Figure 7. The maximum velocity is observed within the furnace near the fuel/oxidizer feeding region. The maximum velocity near the feeding region is about 51 m/s and 36 m/s for the

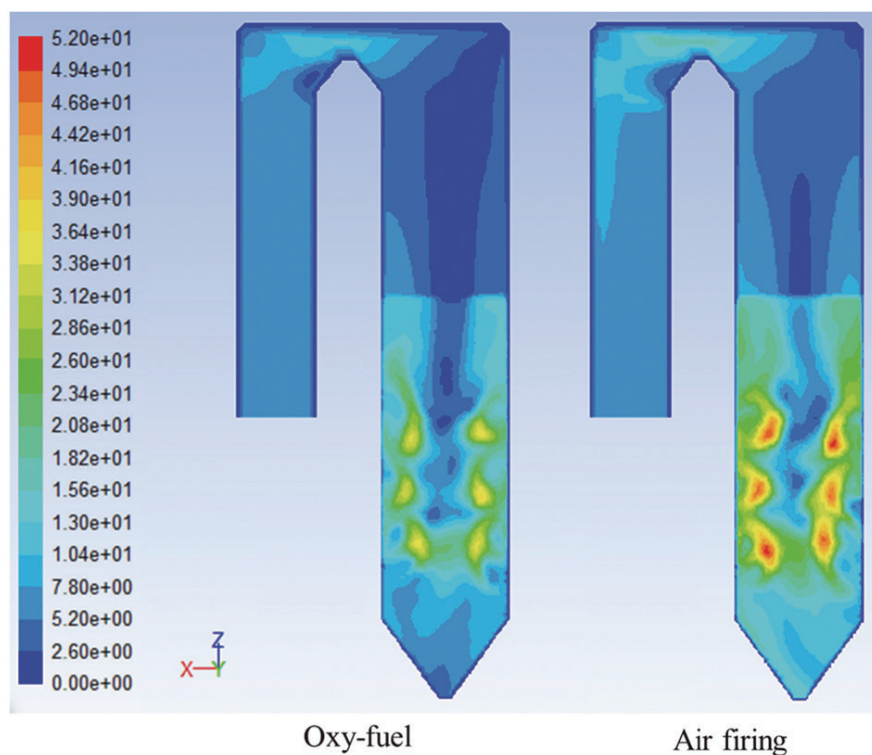


Fig. 7. Velocity distribution of oxy-fuel and air-firing condition (Unit: m/s) (by author).

air-firing and oxy-fuel conditions, respectively. The reduction of the maximum velocity is due to the replacement of N_2 by CO_2 of larger molecular weight for the oxy-fuel combustion condition. However, the variation of the overall velocity within the furnace is not significant. With the tilted injector, the generated vortex leads to long enough resident time for full combustion. With smaller coal particle of PC boiler, the variation of the maximum inlet velocity will not affect the primary performance of the investigated boiler. This may not be valid for the reactor using larger particle of coal for combustion, such as circulating fluidized bed (CFB) reactor. The velocity significantly decreases when entering the heat exchanger due to the momentum sink of the porous effect. Besides the maximum velocity, the overall velocity distributes are similar for both cases.

The high temperature regions (~ 1900 K) are compared in Figure 8. It is observed that the high temperature region concentrates at the central region of the furnace close to Section B and C. The slower inlet velocity and weaker intensity of the

vortex in the oxy-fuel condition leads to a wider higher temperature region than that in air-firing case.

3.3 Detailed distribution in selected regions

Detailed distributions at three selected regions within the furnace are compared in this section. Figure 9 is the schematic diagram. The height is

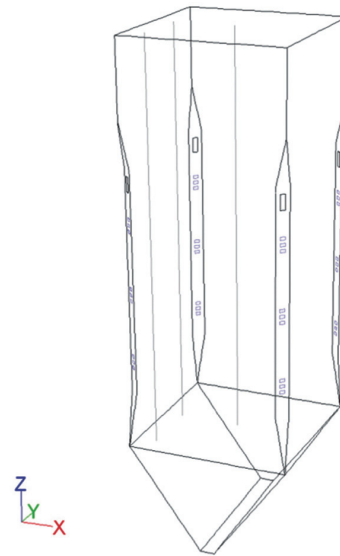


Fig. 9. Three selected vertical lines within the furnace for detailed comparison (by author).

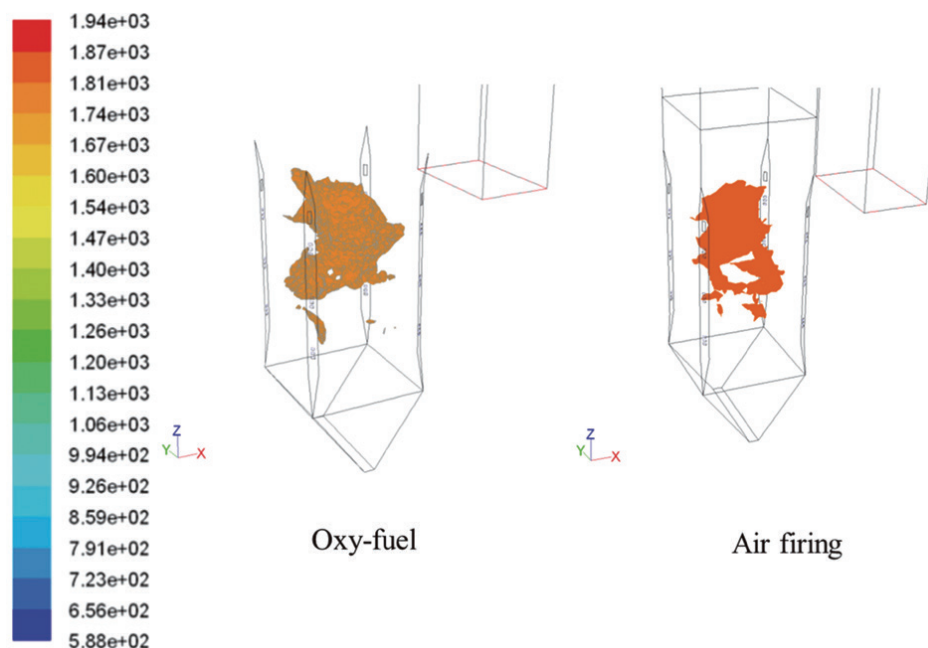


Fig. 8. Comparison of high temperature (~ 1900 K) zones (Unit: K) (by author).

zero at the interface between the top of the hopper and the bottom of the furnace. The temperature, O_2 and CO_2 distribution at corner (Figure 10a), mid-wall (Figure 10b) and center (Figure 10c) are comprehensively compared.

It is shown that the variation near three feeding sections (section A, B, and C) is significant (O_2 increase, temperature and CO_2 decrease) at the corner region (Figure 10a). The extent of variation becomes smaller at the mid-wall region (Figure 10b), and it is minor at the center region (Figure 10c). This trend is due to the vortex flow within the furnace.

The distributions of O_2 for both cases are similar. The peak value can be observed in the position of corner of the inlet sections. For the position of mid-wall and center, the variation is smaller since it is far away from the inlet position. The mole fraction of CO_2 for the oxy-fuel condition varies within 77% ~ 90% (76.7% CO_2 at inlet), while it varies within 0% ~ 20% (0% CO_2 at inlet) for the traditional air-firing condition. Obvious reduction of CO_2 at the inlet section of corner is observed due to the presence of the inlet species. Relatively mild variation can also be observed in the position of mid-wall, and it is insignificant in the position of center. For the region above section C to the exit of the furnace (corresponding to the height from 23 m to 41 m), the distributions of the observed species are relatively stable. There is a

local peak value of temperature after the height of section C, and it decreases with the depletion of oxygen afterward.

The exit temperatures of the furnace are similar, but their variation in section A, B, and C are different. The temperature drop for air-firing at section A is significant (larger than 400 K) when comparing with that of oxy-fuel combustion. Such difference is relatively small in other sections and location (mid-wall and center). Large variation of temperature is observed in the position of corner and mid-wall, and smaller difference is obtained in the position of center region. Although large variation is observed in some regions when switching to the condition of oxy-fuel combustion, the difference of the average outlet temperature of the furnace is only 0.47%. The largest temperatures are also comparable for the case of air-firing and oxy-fuel combustion. Thus, similar thermal results could be kept in the condition of oxy-fuel combustion as desired.

3.4 Comparison of NO_x formation, wall heat flux and temperature

The NO_x formation, wall heat flux for the base case (air-firing) and two additional cases (50/50 and 95/05) are evaluated and compared in Table 7. In the base case (air-firing), the amount of the calculated NO_x formation is consistent with the experimental result (Choi and Kim, 2009). In

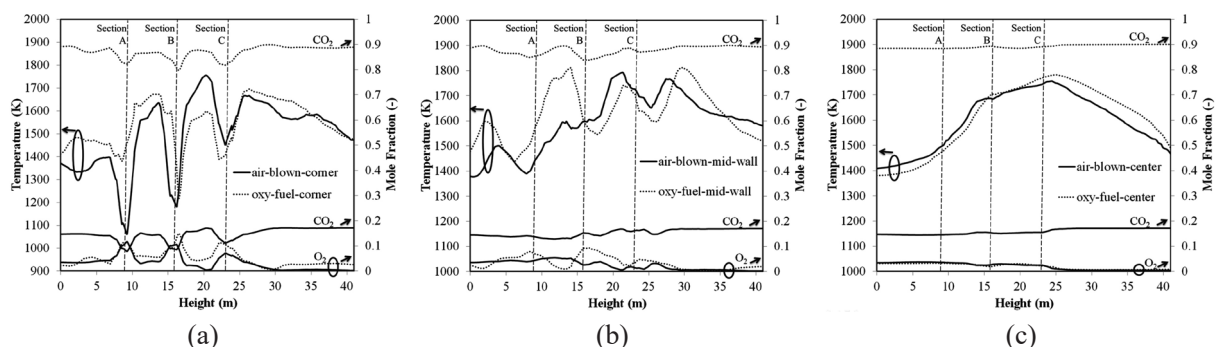


Fig. 10. Comprehensive comparison for three selected region: (a) corner, (b) mid-wall, (c) center (by author).

Table 7. Comparison of NO_x formation and wall heat flux (by author)

Condition	NO _x (ppm) ^a	Wall heat flux (W)
Air-firing (Choi and Kim 2009)	156	5.15E+08
Air-firing (present study)	155	5.28E+08
50/50	108	5.23E+08
95/05	82	5.20E+08

a: raw value.

the case of 50/50, 50% of the nitrogen is replaced by carbon dioxide via the flue gas recirculation, and it is 95% in the case of 95/05. The formation of NO_x decreases when replacing nitrogen by carbon dioxide. The generated NO_x decreases by 30% when switching from air-firing to the case of 50/50. In the case of 95/05, further 24% reduction of NO_x is observed comparing to the case of 50/50. This trend is consistent with the experimental and CFD results of Álvarez *et al.* (Álvarez *et al.*, 2012) and Habermehl *et al.* (Habermehl *et al.*, 2012). Therefore, the oxy-fuel combustion technique is an effective way to reduce the amount of NO_x formation and emission for the PC boiler,

and the present NO_x model is able to reveal it. The wall heat flux slightly reduces by 0.94% when switching to the case of 50/50. For the case of 95/05, a further decrease of wall heat flux is observed (1.5%). Therefore, replacing to the oxy-fuel combustion leads to insignificant drop of the wall heat flux and similar thermal result is kept as desired.

The temperature distributions for three investigated cases are compared in Figure 11. Two temperature distributions of oxy-fuel combustion are similar to that of air-firing. From the air-firing to oxy-fuel combustion, similar thermo results (temperature and wall heat flux) can be kept if the

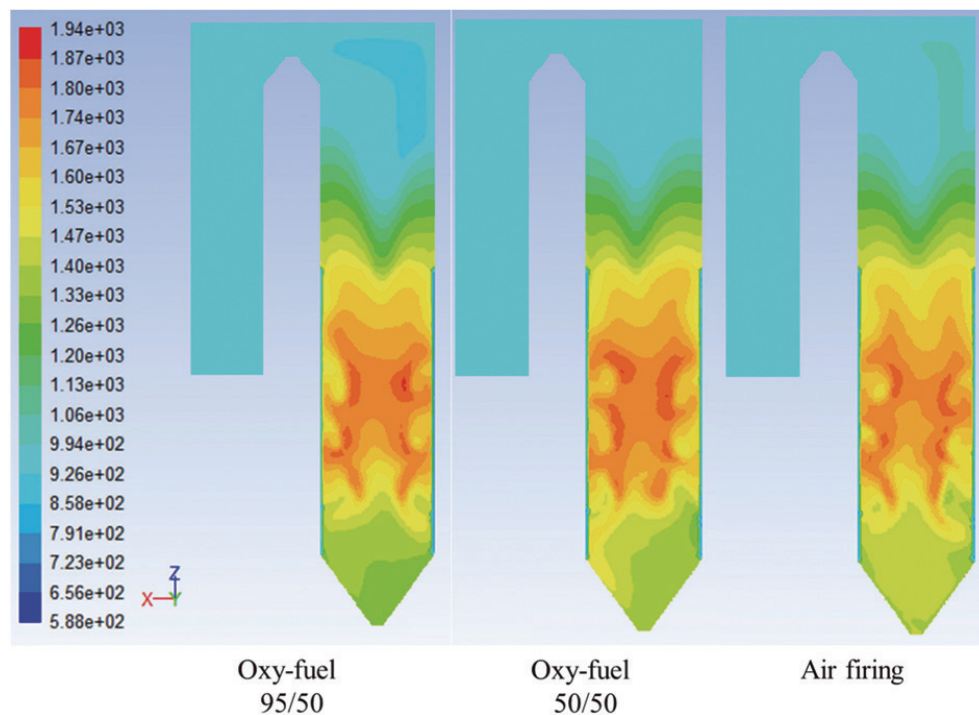


Fig. 11. Comparison of the temperature distribution for the case of 95/05 oxy-fuel combustion, 50/50 oxy-fuel combustion, and air-firing (Unit: K) (by author).

feeding condition is properly changed.

NO_x distributions on the y-mid cross-section for the oxy-fuel and air-firing conditions are presented in Figure 12. The maximum value of generated NO_x is observed within the combustion zone, which is also the position of higher temperature as shown in Figure 11. The variation of NO_x stabilizes when leaving the combustion zone into the heat exchange part. With the reduction of temperature in the heat exchange zone via the absorption of thermal energy, the generated NO_x is not affected until the exit of the boiler. Similar distributions are observed for the compared case with smaller value for the oxy-fuel combustion condition.

4. Conclusion

The effect of oxy-fuel combustion condition on the performance of boiler and NO_x formation is investigated by the proposed numerical model for

a pulverized-coal combustion boiler. Sub-model includes the turbulence model, radiation model and combustion model. The grid system of 0.32 M is adopted since further increase of grid number leads to insignificant variation on the concerned results. The comparison with experimental results showed a consistent trend, validating the proposed numerical model. Furthermore, the condition of oxy-fuel combustion is introduced and results are compared with that of air-firing condition. Results show that the condition of oxy-fuel combustion leads to comparable temperature distribution as desired. Insignificant reduction of wall heat flux is also observed. With larger molecular weight of the introduced CO_2 , the reduction of the maximum inlet velocity and longer resident time are observed.

The generated NO_x via proposed NO_x model is consistent with the reference results. The proposed NO_x model is capable of showing that the oxy-fuel condition is an effective way to reduce the

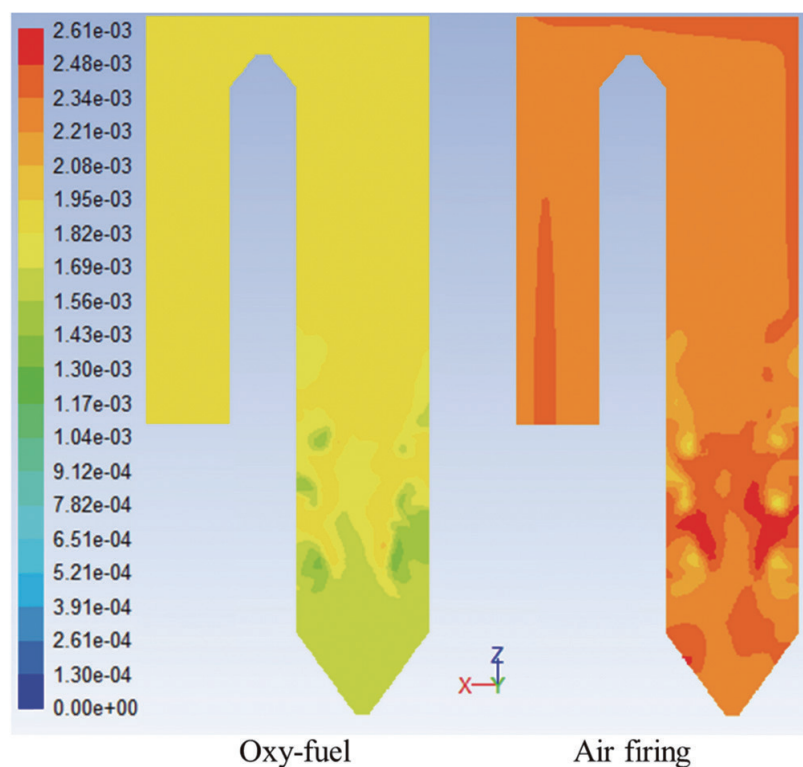


Fig. 12. NO_x distribution of oxy-fuel and air-firing condition (Unit: ppm) (by author).

amount of NO_x formation for the PC boiler. With proper manipulation of feeding condition from air-firing and oxy-fuel combustion, similar thermal related results can be obtained.

References

- Al-Abbas, Audai Hussein, Jamal Naser and David Dodds. 2011. "CFD Modelling of Air-Fired and Oxy-Fuel Combustion of Lignite in a 100KW Furnace." *Fuel* 90(5): 1778-95.
- Álvarez, L., M. Gharebaghi, J. M. Jones, M. Pourkashanian, A. Williams, J. Riaza, C. Pevida, J. J. Pis and F. Rubiera. 2012. "Numerical Investigation of NO Emissions from an Entrained Flow Reactor under Oxy-Coal Conditions." *Fuel Processing Technology* 93(1): 53-64.
- ANSYS. 2013. "ANSYS FLUENT User Manual."
- Arias, B, C. Pevida, F. Rubiera and J. J. Pis. 2008. "Effect of Biomass Blending on Coal Ignition and Burnout during Oxy-Fuel Combustion." *Fuel* 87 (12): 2753-59.
- Backreedy, R. I. L., L. M. A. Mfletcher, Mpourkashanian and A. Williams. 2006. "Modelling pulverised coal combustion using a detailed coal combustion model." *Combustion Science and Technology* 178(4): 763-87.
- Belosevic, Srdjan, Miroslav Sijercic, Simeon Oka and DraganTucakovic. 2006. "Three-Dimensional Modeling of Utility Boiler Pulverized Coal Tangentially Fired Furnace." *International Journal of Heat and Mass Transfer* 49(19): 3371-78.
- Bowman, C. T., 1991. "Chemistry of Gaseous Pollutant Formation and Destruction." In *Fossil Fuel Combustion*, edited by W. Bartok and A. F. Saroffim. John Wiley and Sons, Canada.
- Brunauer, Stephen, 1943. "The Absorption of Gases and Vapors." *Journal of Chemical Education*. American Chemical Society.
- Choi, Choeng Ryul and Chang Nyung Kim, 2009. "Numerical Investigation on the Flow, Combustion and NO_x Emission Characteristics in a 500 MWe Tangentially Fired Pulverized-Coal Boiler." *Fuel* 88(9): 1720-31.
- Chui, E. H., A. J. Majeski, M. A. Douglas, Y. Tan and K. V. Thambimuthu. 2004. "Numerical Investigation of Oxy-Coal Combustion to Evaluate Burner and Combustor Design Concepts." *Energy* 29(9): 1285-96.
- Clements, Alastair G., Sandy Black, JánosSzuhánszki, Katarzyna Stęchły, Alessandro Pranzitelli, William Nimmo and Mohamed Pourkashanian, 2015. "LES and RANS of Air and Oxy-Coal Combustion in a Pilot-Scale Facility: Predictions of Radiative Heat Transfer." *Fuel* 151: 146-55.
- Clements, Alastair G., Rachael Porter, Alessandro Pranzitelli and Mohamed Pourkashanian, 2015. "Evaluation of FSK Models for Radiative Heat Transfer under Oxyfuel Conditions." *Journal of Quantitative Spectroscopy and Radiative Transfer* 151: 67-75.
- Díez, Luis I., Cristóbal Cortés and Javier Pallarés, 2008. "Numerical Investigation of NO_x Emissions from a Tangentially-Fired Utility Boiler under Conventional and Overfire Air Operation." *Fuel* 87(7): 1259-69.
- Edge, P., S. R. Gubba, L. Ma., R. Porter, M. Pourkashanian and A. Williams, 2011. "LES Modelling of Air and Oxy-Fuel Pulverised Coal Combustion—Impact on Flame Properties." *Proceedings of the Combustion Institute* 33(2): 2709-16.

- Fan, Jianren, Ligeng Qian, Yinliang Ma, Ping Sun and Kefa Cen, 2001. "Computational Modeling of Pulverized Coal Combustion Processes in Tangentially Fired Furnaces." *Chemical Engineering Journal* 81(1): 261-69.
- Field, M. A., 1969. "Rate of Combustion of Size-Graded Fractions of Char from a Low-Rank Coal between 1200°K and 2000°K." *Combustion and Flame* 13(3): 237-52.
- Habermehl, Martin, Jens Erfurth, Dobrin Toporov, Malte Förster and Reinhold Kneer, 2012. "Experimental and Numerical Investigations on a Swirl Oxycoal Flame." *Applied Thermal Engineering* 49: 161-69.
- Hanson, Ronald K. and Siamak Salimian, 1984. "Survey of Rate Constants in the N/H/O System BT - Combustion Chemistry." In, edited by William CGardiner, 361-421. New York, NY: Springer New York.
- He, Boshu, Meiqian Chen, Qiumei Yu, Shumin Liu, Lijuan Fan, Shouguang Sun, Jinyuan Xu and Wei-Ping Pan, 2004. "Numerical Study of the Optimum Counter-Flow Mode of Air Jets in a Large Utility Furnace." *Computers & Fluids* 33(9): 1201-23.
- Jones, W. P. and J. H. Whitelaw, 1982. "Calculation Methods for Reacting Turbulent Flows: A Review." *Combustion and Flame* 48: 1-26.
- Jovanovic, Rastko, Aleksandra Milewska, Bartosz Swiatkowski, Adrian Goanta and Hartmut Spliethoff, 2011. "Numerical Investigation of Influence of Homogeneous/Heterogeneous Ignition/Combustion Mechanisms on Ignition Point Position during Pulverized Coal Combustion in Oxygen Enriched and Recycled Flue Gases Atmosphere." *International Journal of Heat and Mass Transfer* 54(4): 921-31.
- Kobayashi, H., J. B. Howard and A. F. Sarofim, 1977. "Coal Devolatilization at High Temperatures." *Symposium (International) on Combustion* 16(1): 411-25.
- Kuang, Min, Qunyi Zhu, Zhengqi Li and Xiang Zhang, 2013. "Numerical Investigation on Combustion and NO_x Emissions of a Down-Fired 350 MWe Utility Boiler with Multiple Injection and Multiple Staging: Effect of the Air Stoichiometric Ratio in the Primary Combustion Zone." *Fuel Processing Technology* 109(x): 32-42.
- Liang, Xiaorui, Qinhui Wang, Zhongyang Luo, Eric Eddings, Terry Ring, Simin Li, Peng Yu, Jiqing Yan, Xudong Yang and Xin Jia, 2020. "Experimental and Numerical Investigation on Nitrogen Transformation in Pressurized Oxy-Fuel Combustion of Pulverized Coal." *Journal of Cleaner Production* 278: 123240.
- Ma, Likun, Xu Huang and Dirk Roekaerts, 2017. "Large Eddy Simulation of CO₂ Diluted Oxy-Fuel Spray Flames." *Fuel* 201: 165-75.
- Millares, Cesar Alfredo Romo, 1992. *Mathematical Modeling of Fuel-NO Emissions from PF Burners*. University of London.
- NETL, 2010. "Advanced CO₂ Capture R&D Program Technology Update."
- NETL, 2012. "Advancing Oxycombustion Technology for Bituminous Coal Power Plants: An R&D Guide."
- Nikolopoulos, Nikos, Aristeidis Nikolopoulos, Emmanouil Karampinis, Panagiotis Grammelis and Emmanuel Kakaras, 2011. "Numerical Investigation of the Oxy-Fuel Combustion in Large Scale Boilers Adopting the ECO-Scrub Technology." *Fuel* 90(1): 198-214.
- OECD, 2010. "Projected Costs of Generating Electricity."
- Porter, R., F. Liu, M. Pourkashanian, A.

- Williams and D. Smith, 2010. "Evaluation of Solution Methods for Radiative Heat Transfer in Gaseous Oxy-Fuel Combustion Environments." *Journal of Quantitative Spectroscopy and Radiative Transfer* 111(14): 2084-94.
- Raithby, G. D. and E. H. Chui, 1990. "A Finite-Volume Method for Predicting a Radiant Heat Transfer in Enclosures With Participating Media." *Journal of Heat Transfer* 112(2): 415-23.
- Sivathanu, Y. R. and G. M. Faeth, 1990. "Generalized State Relationships for Scalar Properties in Nonpremixed Hydrocarbon/Air Flames." *Combustion and Flame* 82(2): 211-30.
- Soete, G. G. De, 1975. "Overall Reaction Rates of NO and N₂ Formation from Fuel Nitrogen." *Symposium (International) on Combustion* 15 (1): 1093-1102.
- Warnatz, J., 2001. "NO_x Formation in High Temperature Processes." University of Stuttgart, Stuttgart, Germany.
- Winter, Franz, Christian Wartha, Gerhard Löffler and Hermann Hofbauer, 1996. "The NO and N₂O Formation Mechanism during Devolatilization and Char Combustion under Fluidized-Bed Conditions." *Symposium (International) on Combustion* 26(2): 3325-34.
- Yang, Xin, Alastair Clements, János Szuhánszki, Xiaohong Huang, Oscar Farias Moguel, Jia Li and Jon Gibbins, 2018. "Prediction of the Radiative Heat Transfer in Small and Large Scale Oxy-Coal Furnaces." *Applied Energy* 211 (August 2017): 523-37.

粉煤鍋爐富氧燃燒特性與氮氧化物生成之數值分析

陳銘宏^{1*}

摘 要

本研究以數值分析方式探討於粉煤鍋爐中進行富氧燃燒程序之現象以及氮氧化物生成評估。所建立之模式主要包括紊流、輻射以及燃燒模式。本模型先經計算網格獨立測試與實驗結果驗證，確立其可靠性後，再進行相關參數分析。比較空氣燃燒與富氧燃燒情況之結果中顯示，富氧燃燒情況將導致相似之溫度分佈、較低之壁面熱傳量、較低之速度與較長之滯留時間。氮氧化物生成評估結果顯示，富氧燃燒條件乃是有效降低粉煤鍋爐氮氧化物生成量之方法。結果亦顯示，在從空氣燃燒切換至富氧燃燒的過程中，藉由適當地改變進料條件，可以維持相似之鍋爐溫度分布。

關鍵詞：數值分析，富氧燃燒，粉煤鍋爐

¹核能研究所機械及系統工程專案計畫 助理研究員

*通訊作者電話: 03-4711400 #3351, E-mail: minghongchen@iner.gov.tw

收到日期: 2020年07月17日

修改日期: 2020年09月07日

接受日期: 2020年09月25日